SUPPORTING INFORMATION FOR:

OPTICAL ENCODING OF LUMINESCENT CARBON NANODOTS IN CONFINED SPACES

Evelyne Bartholomeeusen,[a] Gert De Cremer,[b] Koen Kennes,[c] Ceri Hammond,[d] Ive Hermans,[e] Jiang-bo Lu,[f,g] Dominique Schryvers,[g] Pierre A. Jacobs,[a] Maarten B.J. Roeffaers,[h] Johan Hofkens,[c] Bert F. Sels,[a] and Eduardo Coutino-Gonzalez [i,*]

[a] Chem&Tech - Centre for Sustainable Catalysis and Engineering (CSCE), KU Leuven, Celestijnenlaan 200F, B-3001 Leuven, Belgium.
[b] DSM Protective Materials, PO Box 1163, 6160BD Geleen, the Netherlands.
[c] Chem & Tech - Molecular Imaging and Photonics, KU Leuven, Celestijnenlaan 200F, B-3001 Leuven, Belgium.
[d] Department of Chemical Engineering, Imperial College London, South Kensington, London, SW7 2AZ.
[e] Department of Chemistry & Department of Chemical and Biological Engineering, University of Wisconsin-Madison, 1101 University Av. Madison, WI 53706, USA.
[f] School of Physics and Information Technology, Shaanxi Normal University, Xi'an, 710119, PR China.
[g] EMAT, University of Antwerp, Groenenborgerlaan 171, B-2020 Antwerpen, Belgium.
[h] Chem&Tech - Centre for Membrane Separations, Adsorption, Catalysis and Spectroscopy for Sustainable Solutions, KU Leuven, Celestijnenlaan 200F, B-3001 Leuven, Belgium
[i] Centro de Investigaciones en Óptica, A. C. Loma del Bosque 115, Colonia Lomas del Campestre, León, Guanajuato 37150, Mexico. Email: ecoutino@cio.mx

SI-0 Synthesis and characterization of AFI-type zeolites

Aluminum isopropoxide (Acros), orthophosphoric acid (85 wt %, VWR), tripropylamine (TPA, ≥ 98 %, Acros), ethanol (VWR PROLABO), Aerosil200 (Degussa) and deionized water were employed in the synthesis of AlPO-5 zeolites. In a typical synthesis, the aluminum isopropoxide was dissolved in deionized water, followed by slowly pouring in orthophosphoric acid under continuous stirring at room temperature. After stirring for ca. 20 min, ethanol was added to the reaction mixture. The organic template (TPA, Acros) was then added dropwise and the mixture was stirred at room temperature for an additional 30 min. The molar ratio of Al_2O_3/P_2O_5/TPA/H_2O/EtOH was 1/1/1.3/400/20. The synthesis was performed hydrothermally at 190 °C under a calculated autogenous pressure of 1.3 MPa for 15 to 16 h. During crystallization, the autoclaves were rotated, ensuring effective mixing. The solid was recovered after successively washing with distilled water by centrifugation at 10,000 rpm and dried at 60 °C for 24 h. Scanning electron microscopy (SEM) images of the resulting powder were obtained with a Philips XL 30 FEG. The X-Ray diffraction patterns were recorded on a STOE Stadi P instrument under Cu Kα1 radiation (λ = 154 nm). Thermo gravimetric analysis (TGA) was performed using a Q500 TGA from TA Instruments. During the analysis, the sample was heated up to 800 °C at a rate of 10 °C per minute under a constant oxygen flow of 90 mL/min.

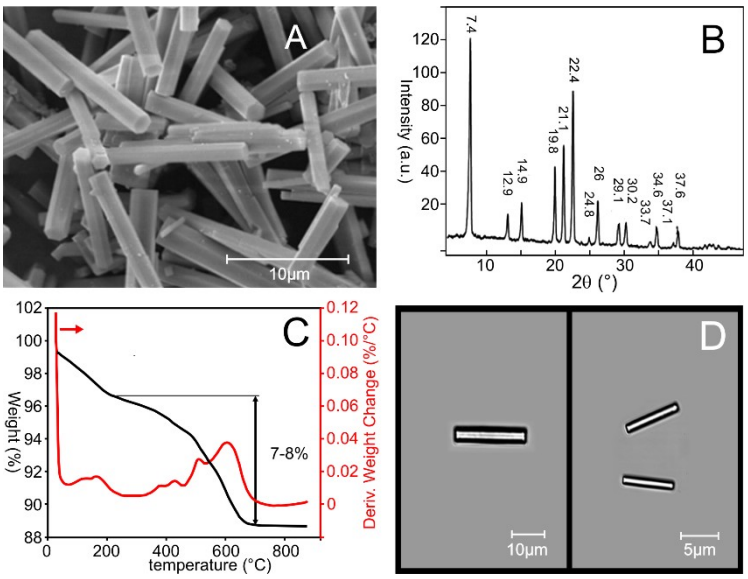

Figure SI-1. Characterization of the AFI-type zeolite including (A) a SEM image, (B) Powder XRD pattern and reflection positions (in 2theta), (C) Thermal gravimetric analysis under oxygen atmosphere for quantifying the amount of template, and (D) Transmission optical microscope images of selected zeolite crystals.

Typical hexagonal crystals of about 10 - 20 µm in length and 1-2 µm in diameter were observed by SEM (Figure SI-1A). A crystalline AFI-type material was identified by XRD analysis (Figure SI-1B). TGA analysis (Figure SI-1C) showed 7 to 8 wt % of tripropylamine (TPA) template molecule, in agreement with the general structure formula of the as-synthesized zeolite. For encoding applications, large individual zeolite crystals were selected, as illustrated in the optical transmission images (Figure SI-1D).

Focused ion beam (FIB) – Transmission electron microscopy (TEM)

The cross-section FIB lamella was prepared with the so-called "lift out" technique using an FEI Helios NanoLab 650 FIB/SEM dual-beam system. An ion-beam-assisted (30kV) protective Pt layer was deposited on the surface of the crystal before FIB cutting. Ga^+ ion beams of 30kV/3nA and 30kV/0.24nA were used for sample cutting and early stage milling. In the final stage, the Ga^+ beam was reduced to 5kV/14pA to minimize ion beam damage during final milling. TEM observations were performed on an FEI Tecnai microscope operated at 80 kV to reduce electron beam damage.

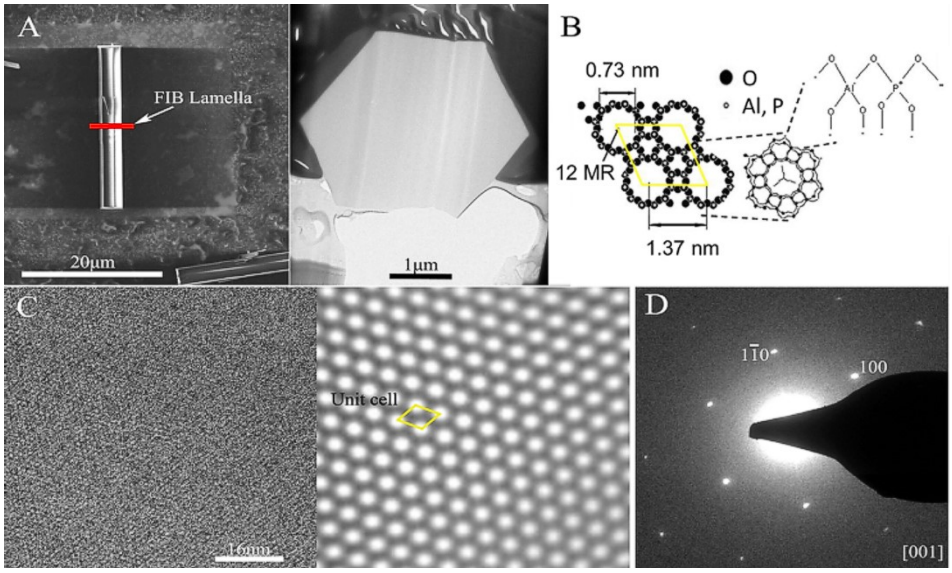

Figure SI-2. Micrographs taken from a FIB lamella of an AlPO-5 crystal. (A) SEM image of a single AlPO-5 crystal and the cross-section of the FIB lamella. (B) Schematic representation of the zeolite framework and unit cell. (C) High resolution-TEM micrograph and the inverse FFT showing the arrangement of the pores. The unit cell is indicated in the enlarged IFFT and (D) corresponding [001] electron diffraction pattern.

SI-I Stability

Stability of the formed fluorescent carbon structures.

The confinement properties of the microporous zeolite host, seem to stabilize the activated carbon species in the zeolite channels, preventing their leaching from the host structure in aqueous environment. This protection also results in a long shelf-life, making the label readable after being exposed to normal atmospheric conditions for at least 3 months (See Figure SI-3).

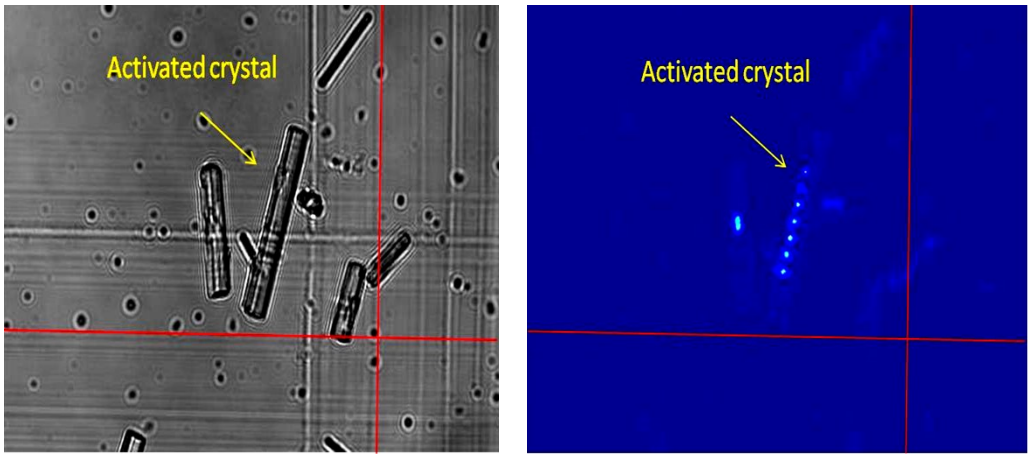

Figure SI-3. Fluorescence image of an activated crystal recorded 3 months after photoactivation.

SI-II Photo-activation experiments

Photo-activation setup description

Encoding and imaging of emissive patterns was performed by photo-activation with a femtosecond pulsed (80 MHz, pulse width ± 100 fs) 780 nm laser (Mai Tai, Spectra Physics). The excitation light was circularly polarized and directed into an oil-immersion objective (Olympus, 1.3 N.A., and 100 x) of an inverted fluorescence microscope (Olympus IX70) using a dichroic beam splitter (680 dcspxr, Chroma). The microscope was equipped with a piezo-controlled scanning stage (Physics Instruments), which was directed by an in-house developed software for writing and imaging the patterns. The typical excitation power for code writing was 9.3 MW/cm². The patterns were imaged using the same setup as described above. The fluorescence was collected by the objective, guided through a 100 µm pinhole and collected onto an avalanche photodiode (SPCMAQ- 15, EG & G Electro Optics). The fluorescence images were obtained using a reduced laser power of 2-4 MW/cm² to avoid further photo-activation during the scanning process. The intensity of the pixels was integrated for 2 ms.

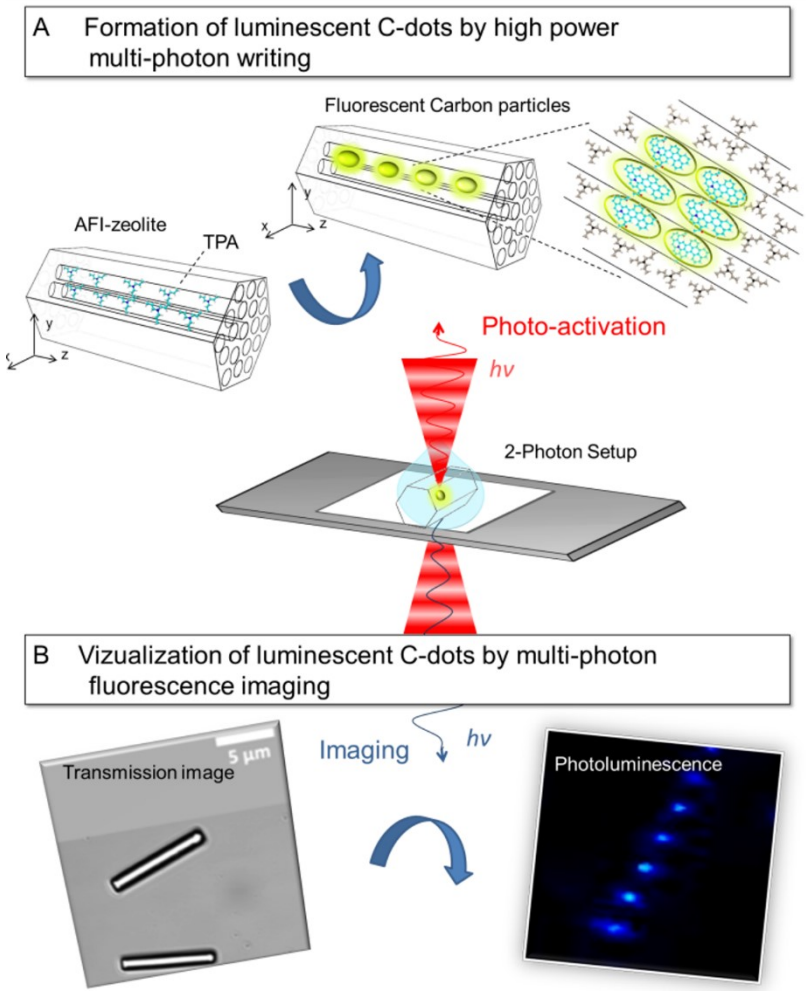

Figure SI-4. Schematic representation of the photo-activation process on an individual zeolite crystal with occluded TPA template molecules, showing the formation (A) and imaging (B) of emissive carbon dot structures. The crystal is immobilized on the glass cover slide and mounted on the confocal fluorescence microscope. Upon intense laser light irradiation zeolite-occluded luminescent carbon nanodots are formed.

Determination of the writing resolution.
For the obtained images after photo-activation the actual writing resolution is significantly lower than the measured FWHM in the final image and even reaches its theoretical limit for two-photon excitation when low laser power (400 kW/cm²) is used. This is visualized by displaying the actual writing resolution in the same graph as the resolution obtained for the image. Note that for an activation time of 2s, the $FWHM_{writing,\,x}$ falling below the theoretical limit is rather the result of fitting inaccuracies.

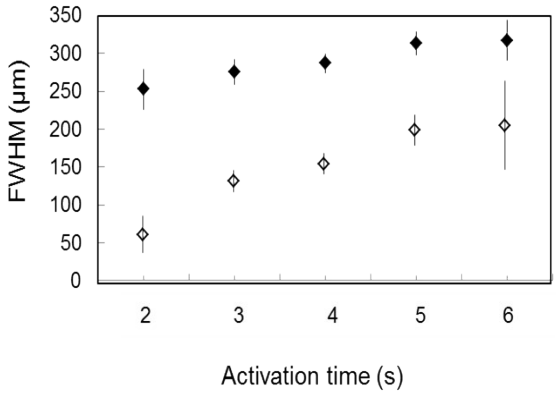

Figure SI-5. FWHM as a function of the activation time. The filled markers give the spot size of the image ($FWHM_{image,x}$). The empty markers show the corresponding real writing resolution ($FWHM_{writing,x}$).

SI-III Confinement and anisotropic growth.

Polarization experiments
The polarization and the stability of the formed emitters were determined by transferring the photo-activated crystals to a Fluoview 1000 confocal fluorescence microscope (Olympus). The fluorescence signal generated by using a polarized 488 nm laser (Spectra Physics) was detected with a photomultiplier tube (PMT) after passing through a dichroic mirror (488 nm) and a 505 nm long pass filter. A 100 µm pinhole ensures a good axial resolution. For measuring the polarization effect, the crystal was rotated over a total angle of 360° in steps of 15° while exciting with a laser beam having a fixed orientation.
The intensity of the emitted light as a function of the activation time is illustrated in Figure SI-6, with the laser polarization direction along (full line) and perpendicular (dashed line) to the pore direction. The difference in intensity indicates that polarization of the emission occurs along the pore direction.

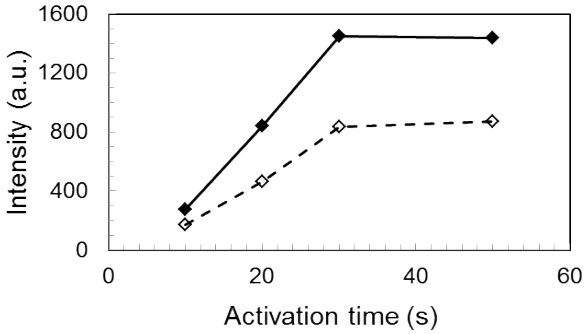

Figure SI-6. The intensity of the emission as a function of the activation time for two polarization angles: 90° (dashed line) and 180° (full line).

The crystal under study was manually flipped over on its side to obtain a better-resolved picture of the former xz-plane, which, after flipping, has become the image plane (xy).

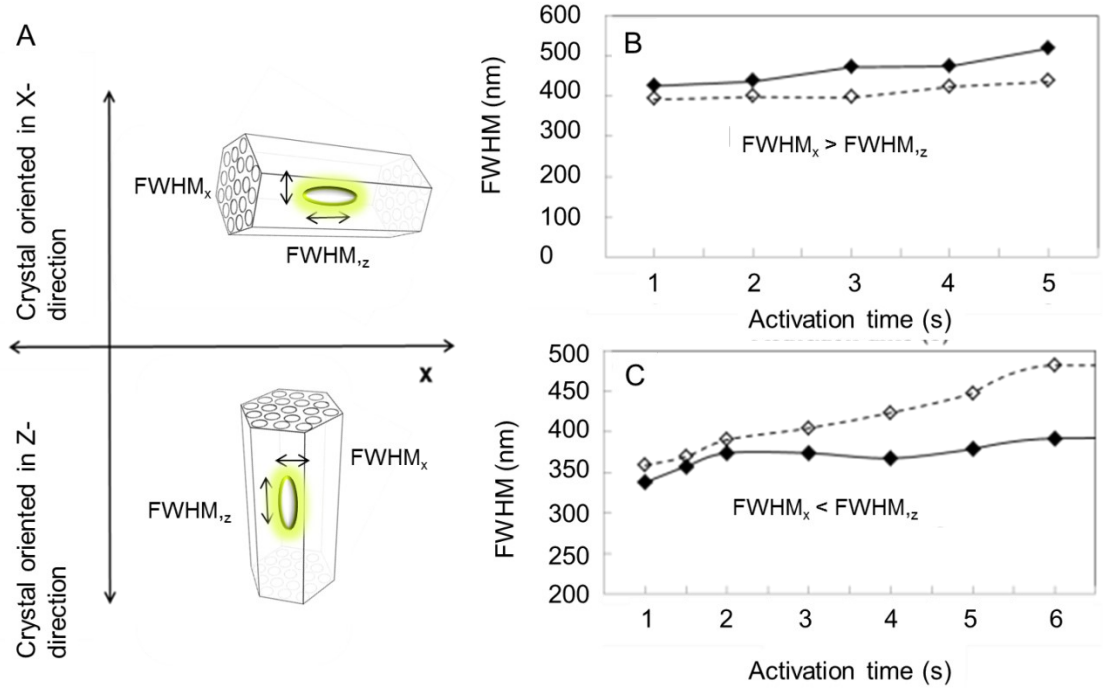

Figure SI-7. (A) Spot size for two zeolite crystals with opposite orientation. FWHM,x (full lines) and FWHM,z (dashed lines) of the spots are given in function of the activation time (B and C).

SI-IV Steady-state characterization.

Emission.

The emission spectra of activated carbon nanodots in AlPO-5 and SAPO-5 are shown in Figure SI-8.

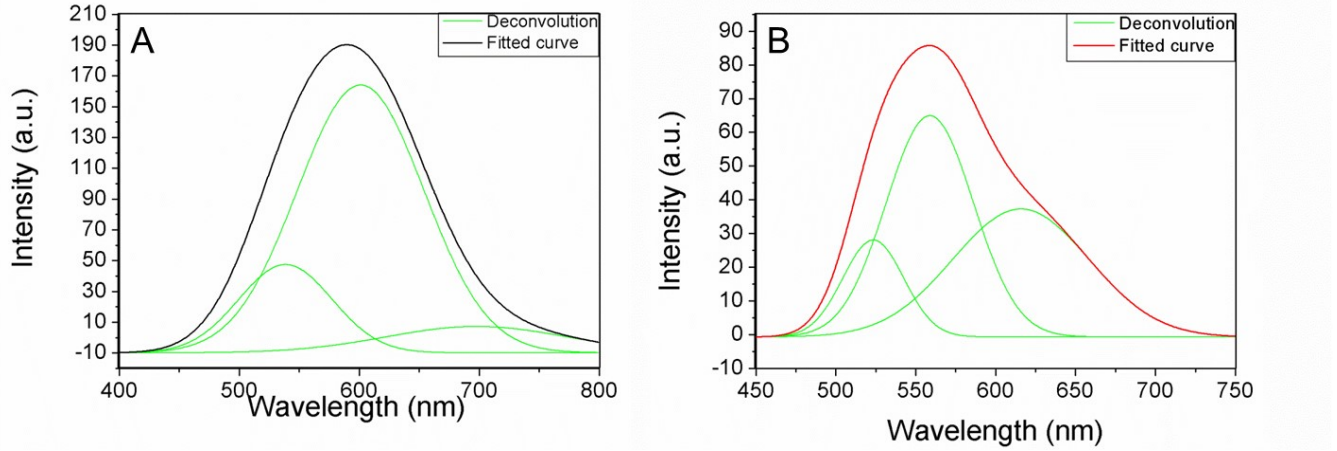

Figure SI-8. Emission spectra (black and red) upon 375 nm excitation with their Gaussian deconvolutions (green) of an activated carbon nanodot in AlPO-5 (A) and SAPO-5 (B).

Deconvolution of the spectra (green), using a Gaussian function, shows that in contrast to AlPO-5 crystals, where an orange fluorescent band around 600 nm is dominant, the Si containing counterpart (SAPO-5) show a shift towards a greenish-yellowish emission with a more pronounced emission band between 523 and 558nm.

Excitation.

The excitation spectra of activated carbon nanodots in AlPO-5 are shown in Figure SI-9.

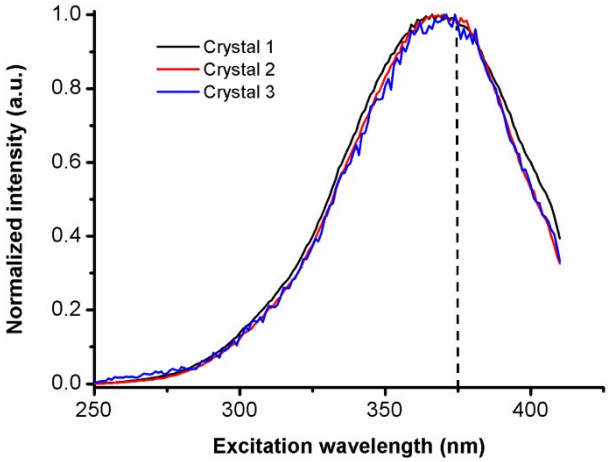

Figure SI-9. Excitation spectra of three different activated AlPO-5 single crystals at 600 nm emission.

Emission wavelength as a function of the activation time.

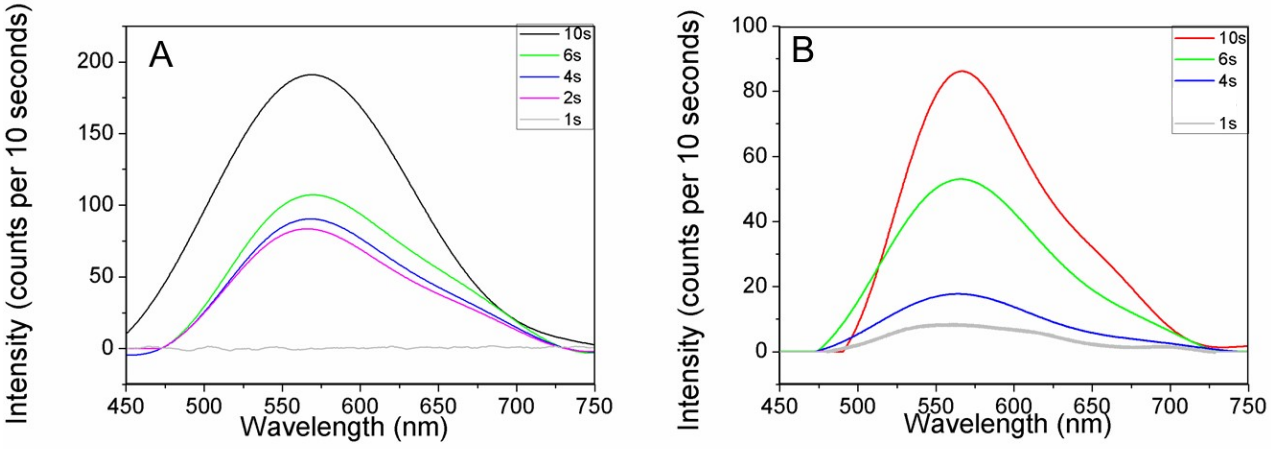

Figure SI-10. Emission spectra of a luminescent carbon nanodot in AlPO-5 (A) and SAPO-5 (B) as a function of the activation time.

Time-resolved measurements in the nanosecond region.

As an excitation light source, the frequency doubled output (375 nm, 8.18 MHz, 0.8 ps FWHM) of a mode-locked Ti:Sapphire laser (Tsunami, Spectra Physics) was used to excite the single crystals. The excitation light, circularly polarized by use of a Berek polarization compensator (New Focus), was directed by using a dichroic beam splitter into the oil-immersion objective (Olympus, 1.3 N.A., 100×) of an inverted microscope (Olympus IX70) equipped with a scanning stage (Physics Instruments). The excitation power was adjusted with a neutral density wheel at the entrance port of the microscope. For the decay measurements at the single crystal level an avalanche photo-diode APD-detector was used in combination with a time correlated single photon counting card (Becker & Hickl,SPC 830). For the decay measurements at specific emission wavelengths, all the fluorescence was collected and focused into a 100-micron multimode optical fiber. The output of the fiber was mounted at the entrance of a double monochromator (Sciencetech 9030, 6 nm bandwith) and the fluorescence was detected with a microchannel plate photomultiplier (MCP-PMT, R3809U, Hamamatsu) connected to the same time correlated single photon counting card (Becker & Hickl, SPC 830). The fluorescent decays were analyzed individually in terms of decay times and their associated pre-exponential factors. The calculated data are given in Table SI-I and SI-II. A graphical representation of the decays in AlPO-5 and SAPO-5 single crystals is given in Figure SI-11. Fluorescein was used as reference for the fittings, having a mono-exponential decay of 3.97 ns (Figure SI.12).

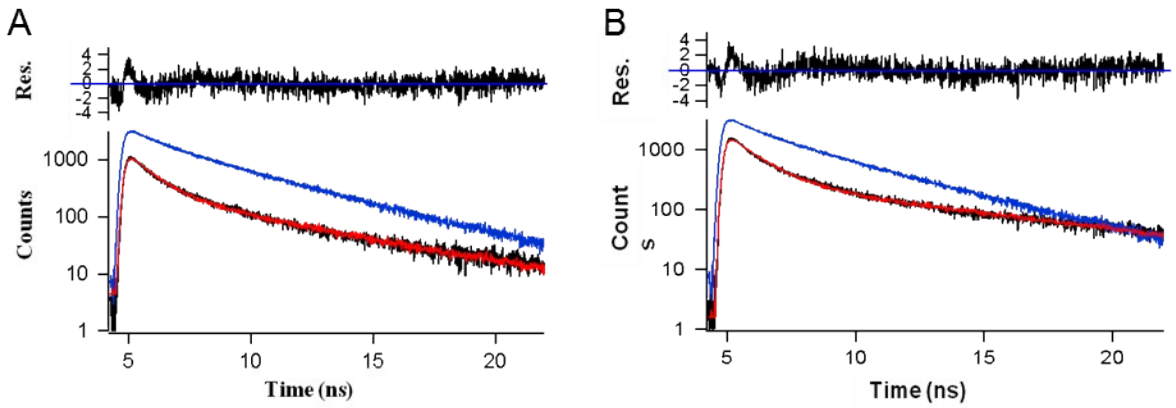

Figure SI-11. Fluorescence decay curves (black line) and fittings (red line) of an emissive spot upon 375 nm excitation for AlPO-5 (A) and SAPO-5 (B). The blue line represents the fluorescein reference. χ^2 varies between 1.002 and 1.096.

The nanosecond decay of fluorescein was measured at bulk level using time-correlated single-photon counting (TCSPC) technique. The frequency-doubled output (375 nm, 8.18 MHz, 2 ps FWHM) of a mode-locked Ti:sapphire laser (Tsunami, Spectra Physics) was used as excitation source. The linearly polarized excitation light was rotated to a vertical direction by the use of a Berek compensator (New Focus) in combination with a polarization filter and directed onto the sample. The emission was collected under 90° with respect to the incident light and guided through a polarization filter that was set at the magic angle (54.7°) with respect to the polarization of the excitation beam. The fluorescence was spectrally resolved by a monochromator (Sciencetech 9030, 6-mm bandwidth), and detected by a microchannel plate photomultiplier tube (MCP-PMT, R3809U, Hamamatsu). A time-correlated single photon timing PC module (SPC 830, Becker & Hickl) was used to obtain the fluorescence decay

histogram in 4096 channels. The decays were recorded with 10000 counts in the peak channel, in time windows of 25 ns corresponding to 6.1 ps/channel and analyzed globally with a time-resolved fluorescence analysis (TRFA) software. The full width at half-maximum (FWHM) of the IRF was typically in the order of 32 ps. The quality of the fits was judged by the fit parameters $\chi 2$ (< 1.2), $Z\chi 2$ (< 3) and the Durbin Watson parameter (1.8<DW<2.2) as well as by the visual inspection of the residuals and autocorrelation function. The fluorescent decays were analyzed individually in terms of decay times and their associated pre-exponential factors.

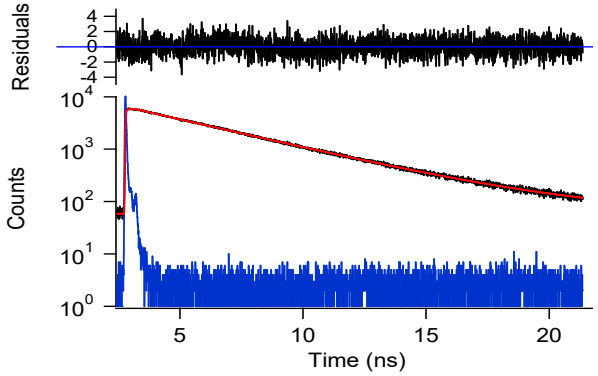

Figure SI-12. Fluorescence decay curve (black line) of fluorescein fitted with a mono-exponential function (red line) and the instrumental response function (blue trace), χ^2 is approximately 1.038.

Table SI-I. Contributions (p) and decay times (τ) upon 375 nm excitation of the different fluorescence-decay components for six activated dots in AlPO-5 with different activation times. χ^2 varies between 1.02 and 1.08.

activation time (s)	τ1 (ns)	p1	τ2 (ns)	p2	τav.(ns)
4	1.1	0.63	4.8	0.37	2.5
5	1.3	0.70	4.7	0.30	2.4
10	1.5	0.71	4.9	0.29	2.5
20	1.3	0.68	4.5	0.32	2.3
40	1.1	0.63	4.1	0.37	2.2
60	1.2	0.62	4.3	0.38	2.3

Table SI-II. Contributions (p) and decay times (τ) upon 375 nm excitation of the different fluorescence-decay components for five activated dots in SAPO-5 with different activation times. χ^2 varies between 1.01 and 1.08.

activation time (s)	τ 1 (ns)	p1	τ 2 (ns)	p2	τav.(ns)
4	1.3	0.66	6.2	0.34	3.0
5	1.4	0.71	5.6	0.29	2.6
10	1.2	0.71	4.4	0.29	2.2
20	1.2	0.68	3.7	0.32	2.0
40	1.2	0.63	4.0	0.37	2.2

SI-V Raman analysis.

A Renishaw inVia Raman microscope using a 325 nm He-Cd laser was employed for the Raman study of the carbon host species. The output was maximized to 20 mW to avoid further activation or destruction of the crystals. The spectrum was obtained by focusing in the most intense fluorescent spot (laser activation time 50 s) of a locally activated zeolite crystal. A background correction was applied by subtracting the Raman spectrum from a point "off the crystal" from the Raman spectrum obtained in the spot. For each measurement, 100 accumulations of 1 s each at a power of 10 mW were employed.

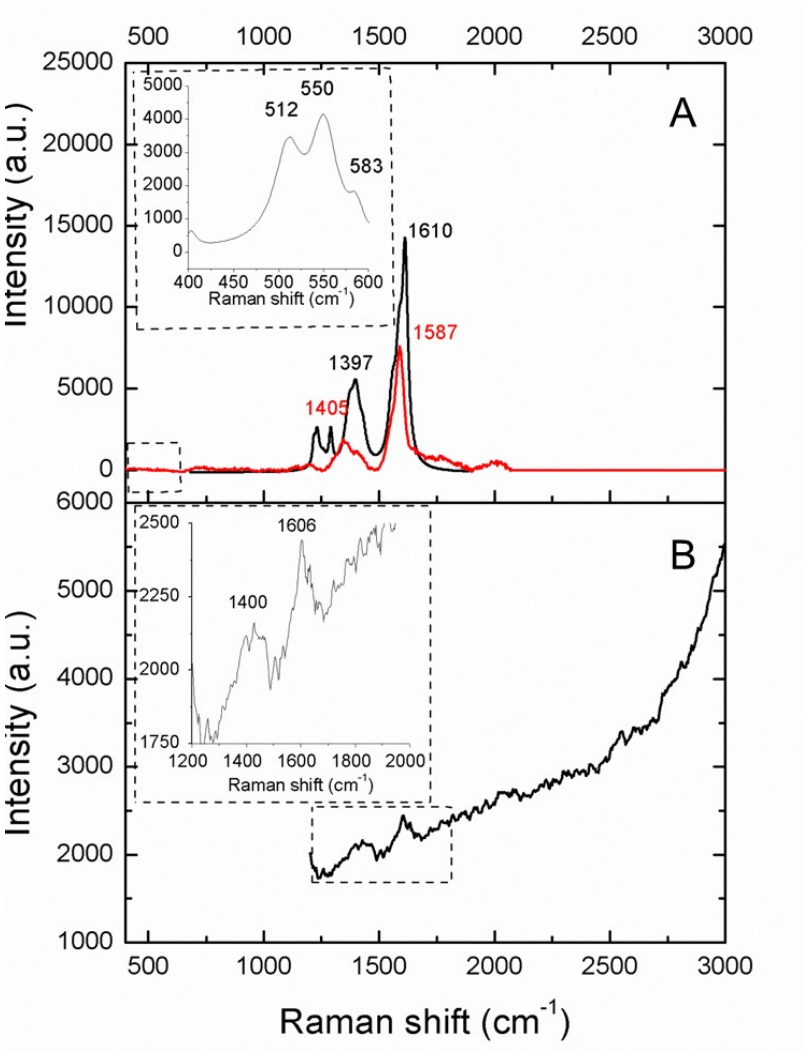

Figure SI-13. Raman spectra of (A) thermally treated AlPO-5 (red) and SAPO-5 (black) samples after pyrolysis at 580 °C and (B) a photo-activated AlPO-5 crystal.

In Figure SI-13A the Raman spectra of thermally treated AlPO-5 and SAPO-5 zeolite samples is displayed, showing the characteristics peaks associated to D (diamond) and G (graphite) carbon structures, at around 1400 and 1600 cm^{-1}, respectively. The radial breathing modes, characteristics of the presence of carbon nanotubes as observed in thermo-activated zeolites powders at low Raman shifts (inset in Figure SI-13A), were not observed at single crystal experiments (Figure SI-13B for AlPO-5 single crystals, the same patterns were also observed in SAPO-5 single crystals), but their complete absence may be due to the low sensitivity of the experiment.